[19]R. D. Puff and J. S. Tenn, Phys. Rev. A 1, 125 (1970).

[20]B. H. Duane (BNW Program LIKELY), U.S. AEC formal document No. BNWL-390, 1967 (unpublished).

[21]χ^2 is defined as the sum of the squares of the differences between theory and experiment weighted by the inverse of the squares of the experimental errors, these errors are derived from counting statistics only. N is the number of independent data points being fitted, reduced by the number of fitting parameters.

[22]K. R. Atkins, *Liquid Helium* (Cambridge U. P., Cambridge, England, 1959).

[23]W. E. Massey and C. W. Woo, Phys. Rev. 164, 256 (1967).

PHYSICAL REVIEW A VOLUME 3, NUMBER 3 MARCH 1971

Experimental Observation of the Drift Dissipative Instability in an Afterglow Plasma

M. W. Alcock and B. E. Keen
United Kingdom Atomic Energy Authority Research Group, Culham Laboratory, Abingdon, Berkshire, England
(Received 1 May 1970)

Measurements are reported on low-frequency self-excited oscillations in an inhomogeneous afterglow plasma, in which there is a radial density gradient perpendicular to an axial homogeneous magnetic field. The plasma was produced either by using a short pulse of electrons emitted from a hot cathode to ionize the background gas, or by pulsing off an rf discharge. The plasma so formed had an initial density of $\sim 10^{10}$ ion cm^{-3} and a temperature $T_e \sim 1000$ °K. The experiment was carried out using tubes of 2.5 and 5.0 cm diam, giving inverse density scale lengths for the radial density gradient of ~ 2.3 and ~ 1.3 cm^{-1}, respectively. The oscillations occurred mainly as $m = +1$ azimuthal modes although some results for $m = +2$ were obtained. The oscillations were shown to be standing waves in the axial direction z with a wavelength λ_z, approximately equal to the column length. It was found that the frequency of oscillation ω was dependent on the column length and by varying this, a dispersion relationship ω vs $k_z = (2\pi/\lambda_z)$ could be plotted under various conditions. It was found that the frequency was independent of time (or density) in the afterglow and that the frequency of oscillation tended to zero as $k_z \to 0$ and to ω^* as k_z assumed larger values. The simple theory of drift dissipative instabilities has been extended to include effects due to electron-neutral and ion-neutral collisions and the Re(ω), and growth rates Im(ω), vs k_z have been calculated for the relevant experimental cases. Comparison of theory and experiment shows remarkably good agreement considering the possible errors in some of the experimental quantities and the assumptions present in the theory.

I. INTRODUCTION

During the last few years there has been much interest in the low-frequency oscillations or instabilities occurring in inhomogeneous magnetoplasmas. This is due to the possible anomalous cross-field diffusion caused by the presence of these microinstabilities. Of particular interest are those instabilities occurring in a plasma with a density gradient perpendicular to the containing magnetic field in the cases where collisions between particles or lack of collisions may lead to oscillations. These self-sustained oscillations are the so-called drift instabilities, and their main properties in both the collisional and collisionless regimes have been summarized by Kadomtsev[1] and Mikhailovski.[2] Unfortunately, in most experiments on drift waves reported to date, large radial electric fields as well as radial density gradients have existed in the plasma. This electric field, together with the longitudinal magnetic field, leads to an azimuthal rotation of the plasma, and consequently causes a Doppler shift in the instability frequency, usually of the same order of magnitude as the drift frequency itself.[3-6] Further, it has been shown[7] that in an inhomogeneous plasma a rotationally convected drift-wave type of instability can be supported if collisions exist in the presence of this radial electric field.

In afterglow plasmas, however, this radial electric field is small (experimentally found to be of the order of 10 mV/cm), and most of the other possible causes of instability such as axial current, nonisotropic velocity distributions, and imposed electric fields are absent. Therefore, most experiments on afterglow plasmas had shown them to be stable, but recently Pigache and Harding[8] have reported the observation of drift waves in a helium afterglow. This paper reports further results obtained in both helium and hydrogen afterglow plasmas on a low-frequency instability. Experiments have been performed in two different tubes, thus varying the density gradient scale length, and in different axial magnetic fields. The instability

frequency was measured as the axial wavelength was varied in each case, and this allowed a dispersion diagram to be constructed. Further measurements were made using a microwave cavity technique[9,10] to determine the electron-neutral collision frequency.

Section II develops the theory of the drift-dissipative instability[11,12] in which both ion-neutral and electron-neutral collisions are included. Section III discusses the apparatus and the diagnostic techniques used to determine the dc properties and the instability characteristics of the plasma. The results obtained using these methods are reported in Sec. IV, and V compares the results with the foregoing theoretical predictions. Finally, it is concluded that good agreement is obtained between the simple theory of the drift-dissipative instability and the experimental results, in view of experimental errors and the approximations in the theory.

II. THEORY

There have been a number of papers recently, which have considered the problem of collisional drift waves in a magnetoplasma. Notable among these was that of Hendel, Chu, and Politzer[5] who achieved a considerable amount of success in applying their linearized theory to the experimental results. In their particular case, the theory was mainly applicable to a fully ionized plasma in which the important collisions for instability were the ion-electron collisions, whereas the stabilizing influence came from finite ion Larmor radius effects and ion-ion collisions. However, in the afterglow plasma considered here, the important collisional times are those concerned with electron-neutral and ion-neutral collisions. A theory of the stability of a gas discharge in a magnetic field with no longitudinal current in the plasma has been developed by Timofeev[11,12] and Kadomtsev.[1]

They have described the plasma behavior by the equations of continuity for the electrons and ions, together with the equations of motion for each of these species. Low-frequency oscillations were considered under the conditions that the plasma was neutral, and thus the ion and electron densities were equal. The equations of continuity were

$$\frac{\partial n_i}{\partial t} + \vec{\nabla}\cdot(n\vec{v}_i) = 0 \quad , \qquad \frac{\partial n_e}{\partial t} + \vec{\nabla}\cdot(n\vec{v}_e) = 0 \quad . \tag{1}$$

The velocities of the electrons and ions $\vec{v}_e$ and $\vec{v}_i$ were found from the equations of motion, in which the electrons were assumed to be inertialess, but the ion motion takes into account inertia and collisions with neutrals. The nonisothermal case $T_e > T_i$ was considered, resulting in the following equations of motion:

$$-T_e\frac{\vec{\nabla}n_e}{n_e} + e\vec{\nabla}\phi - \frac{e}{c}(\vec{v}_e\times\vec{H}) - m\vec{v}_e\nu_e = 0 \quad , \tag{2}$$

$$M_i\frac{dv_i}{dt} = -e\vec{\nabla}\phi + \frac{e}{c}(\vec{v}_i\times\vec{H}) - M_i\vec{v}_i\nu_i - T_i\frac{\vec{\nabla}n_i}{n_i} \quad . \tag{3}$$

Here, $\vec{H}$ is the magnetic field, ϕ is the electric potential, n_i and n_e are the ion and electron density, ν_i and ν_e are the ion and electron collision frequencies with neutrals, respectively, M_i and m are the corresponding masses of ions and electrons, and T_e and T_i are the electron and ion temperatures, respectively.

The above equations were solved under the following approximations:

(i) The slab model was adopted in the localized approximation.

(ii) The equations were linearized to first order for small perturbations of density n, and potential ϕ_1, in which the perturbation was taken in the form $e^{-(\omega t-\vec{k}\cdot\vec{r})}$. Here, ω is the oscillation frequency, and $\vec{k}$ is the wave vector.

(iii) The calculation was considered in the case of oblique propagation to the magnetic field $\vec{H}$ in which it was assumed that

$$k_y \gg k_x \gg \frac{1}{n_0}\left(\frac{dn_0}{dx}\right) \quad .$$

Here, $\vec{H}$ was taken to be uniform in the z direction, while the density gradient was assumed to be along the x direction.

(iv) The low-frequency approximation was considered in which the oscillation frequency $\omega \ll \Omega_i$ ($\Omega_i = eH/M_ic$, the ion cyclotron frequency).

(v) It was assumed that there were no zero-order electric fields present in the plasma (i.e., $\nabla\varphi_0 = 0$), and further that the magnetic field and neutral pressure values were such that $\Omega_i/\nu_i \gg 1$ and that $\Omega_e/\nu_e \gg 1$. Then using the above conditions the electron and ion motion can be considered.

A. Electron Motion

From Eq. (2), zero-order conditions give

$$v_{ex}^0 = -\beta v_e^* \quad , \quad v_{ey}^0 = -v_e^* \quad , \quad v_{ez}^0 = 0 \quad , \tag{4}$$

where

$$\kappa = \frac{1}{n_0}\left(\frac{dn_0}{dx}\right), \; v_e^* = \kappa c T_e/eH \quad , \quad \beta = \nu_e/\Omega_e \quad ,$$

and the 0 superscript refers to zero-order conditions.

First-order equations from the x, y, and z components of Eq. (2) relate the perturbed velocities v_{ex}^1, v_{ey}^1, and v_{ez}^1 with the perturbed density n_e^1 and potential ϕ^1. These are

$$v_{ex}^1 = i\frac{e}{m\nu_e}k_x\phi^1 - \frac{T_e}{m\nu_e}(ik_x-\kappa)\left(\frac{n_e^1}{n_0}\right) - \frac{\Omega_e}{\nu_e}v_{ey}^1 \quad , \tag{5}$$

$$v_{ey}^1 = i\frac{e}{m\nu_e} k_y \phi^1 - i\frac{T_e}{m\nu_e} k_y \left(\frac{n_e^1}{n_0}\right) + \frac{\Omega_e}{\nu_e} v_{ex}^1 \ , \qquad (6)$$

$$v_{ez}^1 = i\frac{e}{m\nu_e} k_z \phi^1 - i\frac{T_e}{m\nu_e} k_z \left(\frac{n_e^1}{n_0}\right) \ . \qquad (7)$$

Substituting these values in the equation of continuity for electrons, and retaining only those terms linear in $\beta = \nu_e/\Omega_e$, there results a relationship between n_e^1 and ϕ^1 which is

$$\left(\frac{n_e^1}{n_0}\right) = \frac{[k_z^2 - i\beta k_y \kappa(1 - \beta k_x/k_y)]}{(D_e k_z^2 - i\omega)} \frac{e}{m\nu_e} \phi^1 \ , \qquad (8)$$

where $D_e = T_e/\nu_e m$ is the diffusion coefficient for electrons.

B. Ion Motion

In a similar manner, from Eq. (3), the zero-order conditions give

$$v_{ix}^0 = \alpha v_i^* \ , \quad v_{iy}^0 = -v_i^* \ , \quad v_{iz}^0 = 0 \ ,$$

where $v_i^* = \kappa c T_i/eH$, $\alpha = \nu_i/\Omega_i$, and the 0 superscript, again, refers to zero-order conditions.

Similarly, the ion equation of motion can be linearized to obtain expressions for v_{ix}^1, v_{iy}^1, and v_{iz}^1. Then, substituting these values into the continuity equation (1) for ions, the following expression relating n_i^1 and ϕ^1 is obtained,

$$\left(\frac{n_i^1}{n_0}\right)\left[\omega + k_1^2\left(\frac{T_i}{M_i}\right)\frac{\omega_1}{\Omega_i^2}\right] = \frac{e\phi^1}{M_i\Omega_i}\left(ik_x\kappa\frac{\omega_1}{\Omega_i} - k_y\kappa - k_1^2\frac{\omega_1}{\Omega_i}\right) \ , \qquad (9)$$

where

$$k_1^2 = k_x^2 + k_y^2 \ , \quad \omega_1 = W + i\nu_i \ , \quad W = \omega - W_0 \ ,$$

$$W_0 = k_y v_{iy}^0 + k_x v_{ix}^0 \ .$$

C. Dispersion Equation

The electron and ion density perturbations n_e^1 and n_i^1 can be eliminated by using the Poisson's equation, $\vec{\nabla}^2\phi = 4\pi ec(n_i - n_e)$. However, in the low-frequency approximation ($\omega \ll \Omega_i$), and assuming the principle of quasineutrality ($n_i^0 = n_e^0$), it can be shown that to the order of approximation in the theory, $n_e^1 = n_i^1$. Then, by combining Eqs. (8) and (9) the dispersion equation relating ω and k can be obtained. This results in the equation

$$W^2 + W\left[W_0 + \frac{x\omega_s}{1+x^2} + i\left(D_e k_z^2 + \nu_i + \frac{\omega_s}{1+x^2}\right)\right]$$

$$- D_e k_z^2 \nu_i + \frac{x\omega_s(\omega^* + W_0)}{1+x^2} + \frac{i\omega_s(\omega^* + W_0)}{1+x^2} = 0 \ , \qquad (10)$$

where the drift frequency

$$\omega^* = k_y\left(\frac{cT_e\kappa}{eH}\right) \ , \quad x = \frac{k_x\kappa}{k_1^2} \ , \quad \omega_s = \frac{k_z^2\Omega_e\Omega_i}{k_1^2\nu_e} \ .$$

The above quadratic dispersion equation can be solved, and expressions obtained for the Re(ω), and the growth rate Im(ω), vs k_z, the axial wavenumber. Substituting the values for the particular conditions that prevail in the experiment, the dispersion equation can be computed in each case. Some of these are shown in Figs 7–11.

III. EXPERIMENTAL DETAILS

A. Apparatus

A schematic diagram of the apparatus used is shown in Fig. 1. A uniform magnetic field is produced in a long solenoid formed by a series of coils each spaced 10 cm apart, producing a uniform magnetic field (~0.5%) in the volume of the plasma over a length of 200 cm. This field could be varied over the range 0.1–3.2 kG. The plasma tube was aligned along the axis of the coils and was usually of borosilicate glass, although for some more critical diagnostic measurements a silica tube was used, as mentioned later in Sec. III B. Two different di-

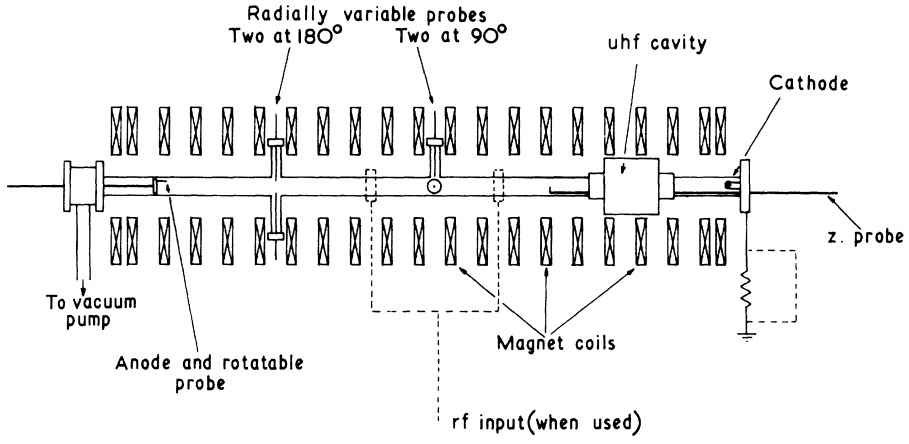

FIG. 1. Schematic diagram of apparatus.

ameter tubes were employed in order that the density gradient scale length could be varied; these were 2.5 and 5.0 cm diam. Neutral gas (hydrogen or helium) was admitted to the tube through an inlet at one end and was allowed to flow through continuously during the course of an experiment. The gas pressure in the tube was monitored by Pirani gauges which were calibrated for the gas in use by means of a McLeod gauge. A combination of leak valve on the inlet side and variable baffle valve on the vacuum pump enabled fine control of the working pressure to be achieved. A variable length of plasma was selected by using a movable anode which slid along the tube and was of finely gridded construction so that it did not impede the neutral gas inflow.

The plasma was formed in two ways: In the first case, a pulsed hot-cathode technique was employed. At one end of the tube a small coiled tungsten cathode was supported, and this was coated with lanthanum hexaboride to increase electron emission and reduce sputtering. This cathode was connected to ground through a small-value resistor (typical value ~ 1 $k\Omega$), and was heated from a half-wave rectified power supply (50 Hz) such that current was only flowing for one-half cycle each period. During the off period, when no current was flowing in the cathode, a highly negative (−500 V) going short pulse (duration 100 μsec) was applied to the cathode (with the anode grounded) thus producing a short burst of electrons which ionized the background gas. The plasma so formed then decayed exponentially for the duration of the "quiescent" period (some 9–10 msec).

The alternative method of plasma production used was a "pulsed-off" rf excited plasma formed between metal straps around the tube and the end plates. This was tried to see if the presence of a hot cathode in the tube was generating undesirable effects (such as "hot" electrons, longitudinal electric fields, etc.) which might be the cause of the instability in this apparatus. As will be shown in Sec. IV, there was no difference in the dispersion curve obtained by this production technique over that obtained when using the hot-cathode method. The outline of this rf excitation method is shown dotted in Fig. 1.

B. Diagnostic Techniques

1. *Probes*

At the center of the tube were two ports, 180° apart, and at one-quarter the tube length was another pair at 90° apart azimuthally. Interchangeable probes could be inserted at each of these ports, and were movable so that they could be set in any radial position. A longitudinally movable probe was inserted from the cathode end and could be moved over two-thirds the length of the tube. The tip of the probe was formed at 90° to the body by a tungsten wire sealed through the glass exterior with a position at $\frac{1}{2}a$ (a is the tube radius). Another similar probe was mounted directly at the periphery of the anode and could therefore be rotated through the full 360° in order to detect the azimuthal variation of the instability. Since the plasma under investigation was an afterglow it was necessary to make fairly accurate time-resolved measurements in the decay, and it was essential therefore that the probes had a short time constant. Typically, a probe circuit time constant of 10^{-5} sec was used.

2. uhf *Cavity*

A cylindrical cavity (15 cm diam, 10 cm long) operating in the TM_{010} model was mounted on the tube. At each end of the cavity were short cylinders (4 cm long) closely fitting the plasma tube, which acted as waveguides beyond cutoff at the resonant frequency (1320 MHz). The cavity was made from solid brass split longitudinally to eliminate joints in the walls running across the direction of current flow for this mode. The smaller plasma tube was made of silica thus enabling a cavity $Q \sim 5000$ to be achieved. Maximum power transmission was observed at resonance, the power level used being set to a minimum. The frequency was measured with an electronic counter. The cavity was used either to measure the average density, or to estimate the electron collision frequency.

To measure the density the resonant frequency of the cavity without plasma was first found (f_0). The oscillator was then reset to a new frequency corresponding to a cavity resonance when a plasma of average density n(t) was present. The change in frequency Δf corresponding to a change in average density, has been computed by a perturbation analysis method for values of $f_0 < f_p$ {where $f_p = [4\pi n(t)e^2/m]^{1/2}$ is the plasma frequency for that particular density $n(t)$}. This analysis led to a relationship of the form[13]

$$\Delta f/f_0 = F_r (r_1/r_2)^2 (f_p/f_0)^2 \quad , \tag{11}$$

where F_r is a form factor dependent on the geometry of the cavity and plasma and r_1 and r_2 are the radii of the plasma and cavity, respectively. Curves of this function F_r are shown in the paper by Agdur and Enander[13] for the various cavity modes of oscillation, thus with this knowledge $n(t)(\propto f_p^2)$ can be obtained.

If losses in the plasma are taken into account by including a collision frequency ν_e for the electrons, the change in Q value of the cavity with and without the plasma present can be written[10] as

$$1/Q - 1/Q_0 = \nu_e \Delta f/\pi f_0^2$$

or alternatively,

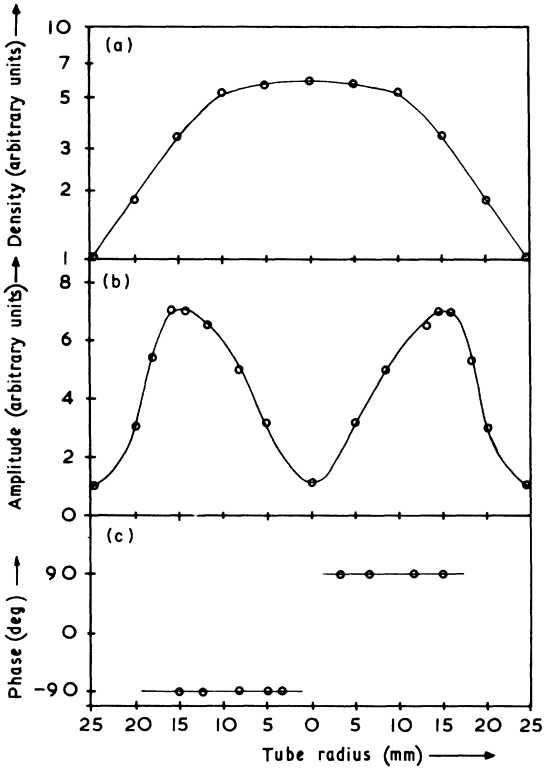

FIG. 2. (a) Density profile, (b) amplitude variation, and (c) phase variation, as a function of radial position. These were taken from a hydrogen plasma in the larger-diameter tube in a magnetic field $H = 175$ G and a neutral pressure of 10 mTorr at a time of 2 msec in the afterglow.

$$\nu_e = \frac{\pi f_0^2 \Delta(1/Q)}{\Delta f} , \tag{12}$$

where Q_0 is the unloaded Q value of the cavity. Hence measurements of the change in Q of the cavity together with the frequency difference can lead to a value for ν_e.

IV. RESULTS

A. Zero-Order Measurements

As was mentioned in Sec. III, the density was determined using the uhf cavity method, but this technique only allowed a determination of the mean density averaged over the cross section of the plasma. Consequently, in order to determine the density profile across a radius of the column, a single-probe technique was used. The ion saturation current $i_s(r)[\alpha n(r)]$ to the single probe was measured at a fixed time τ in the afterglow as a function of radial position. A typical profile for the larger tube is shown in Fig. 2(a) taken in a H_2 plasma at a neutral pressure of 10 mTorr., axial magnetic field $H = 175$ G, and a time 2 msec in the afterglow. It is seen that the inverse scale length, in this case

$$\kappa = \frac{1}{n_0} \frac{dn_0}{dr} \approx 1.3 \pm 0.1 \text{ cm}^{-1},$$

is constant over the radial range 1.3–2.5 cm. It was checked that similar reduced density profiles were obtained for various times $\tau > 1$ msec in the afterglow, and at various positions along the plasma. Also, as the length of the plasma was varied similar profiles were measured.

The electron temperature T_e and ion temperature T_i are extremely difficult parameters to measure, and at first sight it might be supposed that these temperatures could be assumed as ambient, but a close study of the literature reveals that although this should be true for the ions, the evidence suggests that elevated electron temperatures can exist for several msec into the afterglow.[14–17] Some effort has been expended on this measurement using a single probe. However, the use of probes in low-density plasmas in a magnetic field presents some difficulty, a discussion of which is given by Chen.[18] Fortunately, the temperature is one measurement which is least disturbed under these conditions, provided that conditions for making a valid probe measurement are appreciated. These are that the current drain must be kept to an absolute minimum while a short enough response time of the probe is retained. The drain problem is a serious one and inevitably will eventually affect the characteristic as the current is taken nearer to the electron saturation value. This limits the portion of the probe characteristic which is useful, to that part from the ion saturation current, to some limiting value of electron current well short of electon saturation. This useful part of the curve represents electron current drawn mainly from the high-energy tail, and thus electron temperatures based on the concept that the electron velocity distribution is Maxwellian would be in error if this condition was not satisfied. Similar reasoning applies to the use of an equal-area double probe which in all cases samples this portion of the probe characteristic. However, unless one supposes a unique combination of parameters changing in the appropriate manner to achieve the same effect, the fact that a nearly constant frequency with time is observed experimentally suggests that the temperature does not change rapidly during this period (i.e., from 2–6 msec after start of the decay). Measured temperatures within this period gave values between 800 and 1200 °K, and thus a value of 1000 °K was taken for calculation purposes. A typical semi-logarithmic plot of electron current I_e against applied potential V_p is shown in Fig. 3.

The measurement of electron-neutral collision frequency ν_e was made possible by noting the change in Q of a resonant cavity. This cavity, basically designed to measure the electron density, had a Q

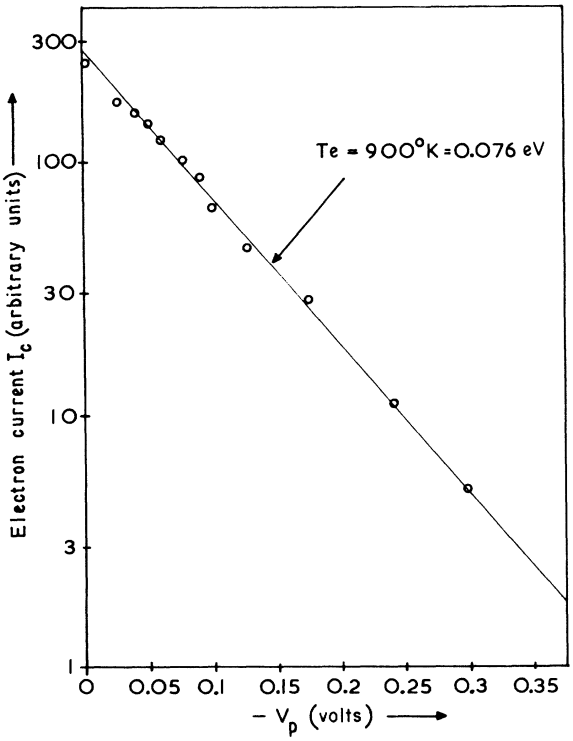

FIG. 3. Semilogarithmic plot of electron current i_e vs applied voltage V_p to a single probe in a plasma.

of 5000 when used with a silica discharge tube. Two possible methods were available as follows:

(i) One method measured the change in Q produced as the resonant frequency with the plasma present was varied from $\Delta f = 0$ up towards the plasma frequency ω_p, where collisional effects increased. This is the method outlined in Sec. III.

(ii) The other used a fixed offset frequency and measured the change in $(1/Q)$ as a function of neutral pressure p. This should give a linear relationship, and when the Q has been reduced to a small fraction of its initial value, gives a reliable result.

Both methods have been used and give good agreement. A plot of $(1/Q)$ vs pressure is shown in Fig. 4(a) for a hydrogen plasma and in Fig. 4(b) for a helium plasma. It is assumed that the measured electron collision frequency is indeed the electron-neutral collision frequency since $(1/Q)$ is, in fact, linearly proportionally to the neutral pressure over a reasonable range of pressure. The final values of (a) $\nu_e/p = (0.70 \pm 0.15) \times 10^9$ sec^{-1} Torr^{-1} for the H_2 plasma and (b) $\nu_e/p = (0.80 \pm 0.15) \times 10^9$ sec^{-1} Torr^{-1} for the He plasma were adopted as those to be used in the experiment.

The ion-neutral collison frequency proved to be an extremely difficult parameter to measure, and as a consequence, its value was estimated from theoretical comparison with the measured electron-neutral collision frequency. From simple kinetic theory considerations, the ratio of the collision frequencies ν_i/ν_e can be related to the collision cross sections S_1 and S_e and their collisional velocities v_i and v_e (where v_i and v_e are the thermal velocities of ions and electrons, respectively). The relationship is $\nu_i/\nu_e = v_i S_i / v_e S_e$. On the solid-sphere approximation, if the ion diameter is assumed to be much greater than the electron diameter, and of the same order as the neutral-particle diameter, $S_i/S_e = 4$. Hence, from a knowledge of the electron and ion temperatures T_e and T_i, respectively, the ion collision frequency can be obtained. This gave (a) $\nu_i/p = (2.0 \pm 0.15) \times 10^7$ sec^{-1} Torr^{-1} for the He plasma and (b) $\nu_i/p = (2.5 \pm 0.15) \times 10^7$ sec^{-1} Torr^{-1} for the H_2 plasma (H_2^+).

B. Instability Measurements

The instability was observed as a decaying sinusoidal oscillation from a single probe in the plasma when the magnetic field and neutral gas pressure had been optimized. A typical oscillating decay signal is shown in Fig. 5, where the output from two single probes separated azimuthally by 180° are presented. The properties of the oscillation were found as follows in Secs. IV B 1–IV B 5.

1. *Azimuthal Variation*

The azimuthal variation in phase was observed by comparing the phase of the signal from the ro-

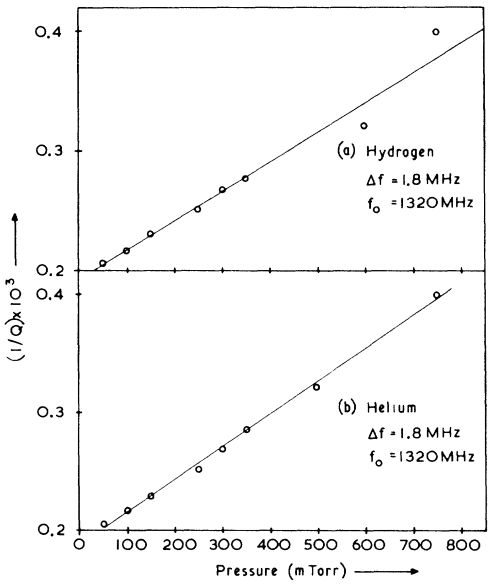

FIG. 4. Change in $1/Q$ of the cavity as a function of neutral pressure for (a) a hydrogen plasma and (b) a helium plasma.

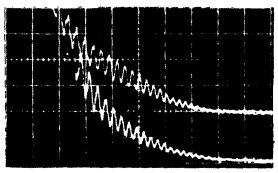

FIG. 5. Typical decay curves for the instability, showing the output from two single probes separated azimuthally by 180°.

tatable probe with that of one of the fixed probes. The amplitude was also measured on this rotatable probe. The azimuthal and amplitude variations were consistent with an azimuthal propagating wave, with either an $m = +1$ or $m = +2$ mode. Each was observed separately under different conditions.

2. *Radial Variation*

The variation in amplitude and phase was measured on a radially movable single probe. The smallest of the available probes was used in order to minimize any disturbance of the plasma, although the use of a large probe made no apparent difference. The resulting amplitude and phase variation was consistent with a $m = +1$ or $m = +2$ propagating wave, under the appropriate conditions for either mode. Plots of the amplitude variation and the phase variation for an $m = +1$ mode as a function of radius are shown in Figs. 2(b) and 2(c), respectively. This also was taken in the hydrogen plasma at $H = 175$ G and $p = 10$ mTorr.

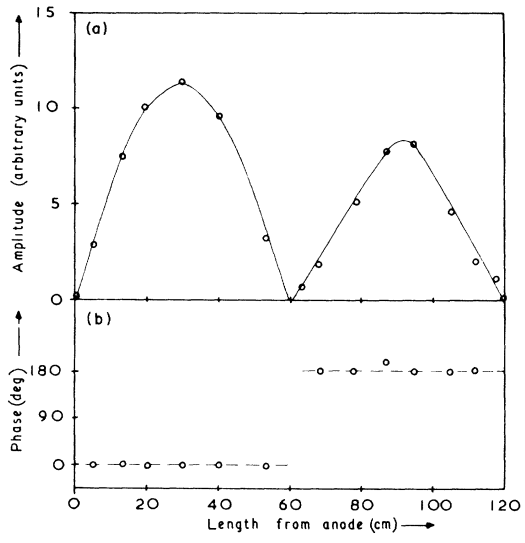

FIG. 6. (a) Amplitude variation and (b) the phase variation as a function of axial length, for $m = +1$ azimuthal mode instability.

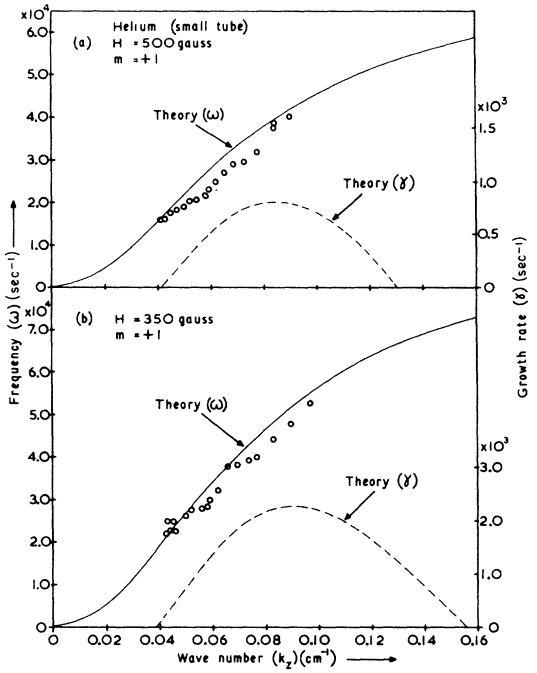

FIG. 7. Dispersion diagram for a helium plasma at (a) $H = 500$ G and (b) $H = 350$ G.

3. *Longitudinal Variation*

The longitudinal variation of amplitude and phase was observed using the axially movable probe. This was checked at various plasma lengths, obtained by moving the position of the anode. Typical results are shown in Fig. 6(a) for the amplitude and in Fig. 6 (b) for the phase taken over a plasma length of 120 cm. The deduction from these results is that the basic configuration in the tube is a standing wave in the axial direction, with a wavelength approximately equal to the plasma length. This is in contrast to other drift-wave experiments[5] where one half-wavelength in the tube has been observed.

4. *Dispersion Relationship*

The frequency of the instability at any plasma column length was determined from oscilloscope display photographs of the decaying signal, as shown in Fig. 5. By displaying the output from two probes 180° apart, a constant check can be kept that the mode number is constant. This procedure was adopted as the plasma length was varied, consequently allowing a ω-k dispersion diagram to be obtained. Experiments were first performed using the small-diameter tube and the hot-cathode plasma-production technique. The magnetic field and neutral pressure were varied until optimum values were obtained. These conditions were then maintained constant throughout a series of experiments. Typical results are shown in Figs. 7(a) and 7(b) for

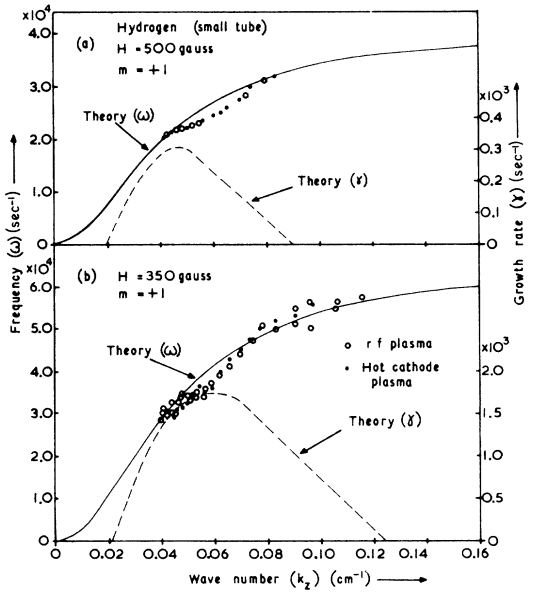

FIG. 8. Dispersion diagram for a hydrogen plasma at (a) $H = 500$ G and (b) $H = 350$ G.

experiments performed in a helium plasma at the magnetic fields of $H = 500$ G and $H = 350$ G, respectively. Results obtained using a hydrogen plasma are shown in Fig. 8 for the same magnetic fields.

As a check to obviate any effect due to the presence of the hot cathode in the plasma tube, a discharge was struck using a 27-MHz rf oscillator to produce the plasma. The afterglow was produced by "pulsing off" this oscillator for ~ 20 msec. Very similar results were obtained as can be seen by comparing the results obtained by the differing plasmas in Fig. 8.

As a further check, a larger-diameter discharge tube was tried, as this approximately halved the radial scale length. Under these conditions, with $H = 175$ G, it was possible to obtain $m = +1$ and $m = +2$ modes in the tube, separately, as the plasma length was varied. The results are shown in Fig. 9 for a helium plasma and in Figs. 10(a) and 10(b) for a hydrogen plasma for $m = +1$ and $m = +2$ azimuthal modes, respectively.

In Figs. 7–10, the solid line shows the theoretically computed Re(ω)-vs-k_z curve using the theory developed in Sec. II and refers to the left-hand scale. The theoretical growth rate γ is shown as the dashed curve in the figures and refers to the right-hand scale.

5. *Frequency Variation as a Function of Neutral Pressure*

In principle, it would have been desirable to measure the frequency variation as a function of both the axial magnetic field $\vec{H}$ and of the neutral pressure, at constant axial wave number k_z for each gas. As soon as the magnetic field was varied, the inverse density scale length "κ" changed and so did the perpendicular wave number $k_\perp$. Therefore, in order to compare measured values of frequency as a function of magnetic field with the theoretically predicted values, it would have been necessary to measure κ and $k_\perp$ at each magnetic field value. However, it was possible to obtain measurements in the larger tube, while the neutral pressure was varied over a reasonable range of pressures, for both gases. These experiments were performed with a constant axial wave number ($k_z = 0.04$) and at two values of magnetic field $H = 175$ G and $H = 250$ G. As the pressure was varied, the inverse scale length κ and the wave number $k_\perp$ both remained relatively constant over the pressure range employed.

Figure 11 shows the experimental results obtained for both the helium and hydrogen plasmas. The solid line shows the theoretically predicted variation of frequency as a function of neutral pressure in each case, calculated for the conditions when $H = 175$ G. The predicted variation for the conditions when $H = 250$ G is almost identical and thus has not been marked separately. The dashed curve shows the predicted variation of the growth rate [$\gamma = \mathrm{Im}(\omega)$] as a function of pressure and refers to

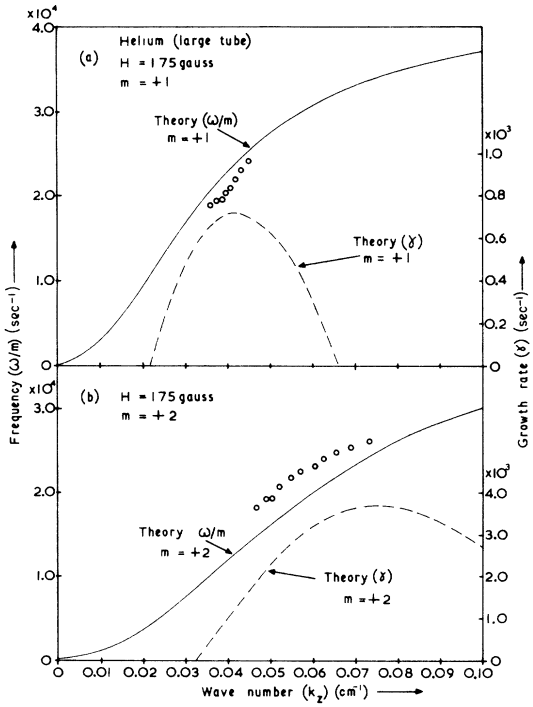

FIG. 9. Dispersion diagram for a helium plasma in $H = 175$ G for (a) $m = +1$ and (b) $m = +2$ azimuthal mode number.

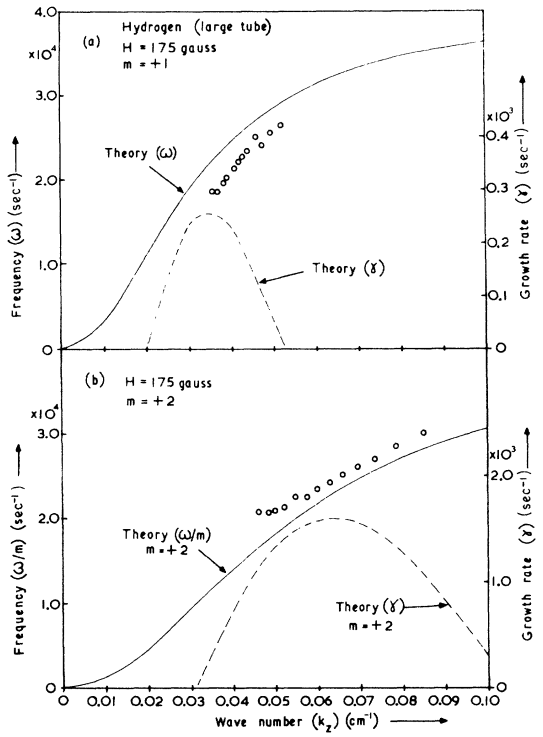

FIG. 10. Dispersion diagram for a hydrogen plasma in $H = 175$ G for (a) $m = +1$ and (b) $m = +2$ azimuthal mode number.

the right-hand scale in each case.

V. DISCUSSION AND CONCLUSIONS

In Sec. II, the stability conditions for an inhomogeneous plasma in a magnetic field were investigated using slab geometry. It was shown that if electron-neutral as well as ion-neutral collisions were taken into account, an instability could be present in the plasma at certain wavelengths. In order to compare the experimental results obtained on a cylindrical plasma column, with these theoretical predictions, certain qualifications have to be made:

(i) The cylindrical case has been approximated by taking over the Cartesian coordinate calculation by assuming that $x \to r$, $y \to r\theta$, and $z \to z$. In this way $k_y \to m/r_0$, where r_0 is taken as the radius at which there is a maximum in the instability amplitude and m is the azimuthal mode number associated with the mode. A condition for this approximation is that the azimuthal wave number k_y should be large compared with the inverse scale length κ (i.e., $r_0\kappa/m \ll 1$). Experimentally, $r_0\kappa/m \approx 1$ is the worst case, and this is a point of divergence between theory and experiment. Recently, however, Chu, Coppi, Hendel, and Perkins[19] have performed a calculation for collisional drift waves in cylindrical geometry, and they comment that the dispersion relationship so obtained has almost the same form and coefficients as the "local" slab model dispersion relationship. Therefore it appears that, perhaps, this is not such an important point of divergence.

(ii) The theory developed in Sec. II is a small amplitude linearized theory, where the potential and density perturbations are assumed to be a small percentage of the zero-order values. In fact, any instability must have grown to an amplitude value which is limited by nonlinear terms not included in the theory, and in this experiment, values up to $n_1/n_0 \approx 25\%$ have been observed. However, some nonlinear mechanisms[20,21] may limit the final instability amplitude so that the observed mode phenomena are closely related to the unstable perturbations predicted by the linear theory.

(iii) Another important feature is that the slab model is based on the "local" approximation. A more realistic calculation would be to evaluate the dispersion equation from the equations of motion in cylindrical geometry with the appropriate boundary conditions taken into account. Then the solution to the eigenvalue problem could be used to examine the stability of the plasma. The "local" approximation can only be justified under the condition $\kappa r_0 \ll 1$. As mentioned previously, this is not the case experimentally.

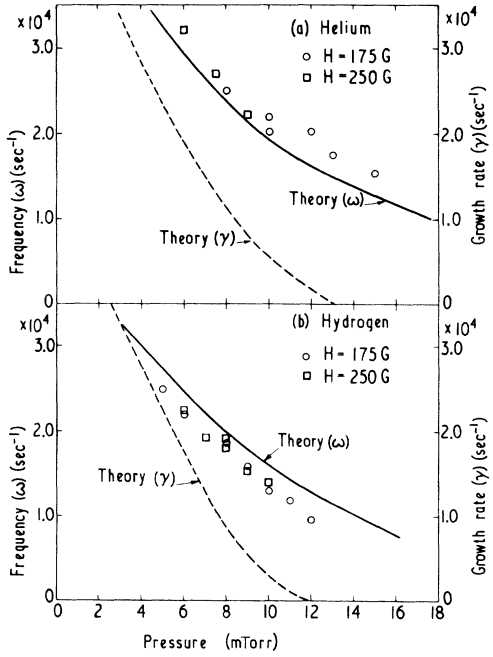

FIG. 11. Measured values of frequency as a function of neutral pressure in (a) a helium plasma and (b) a hydrogen plasma, obtained in magnetic fields of $H = 175$ G and $H = 250$ G.

(iv) Other approximations involved are $\nu_i/\Omega_i \ll 1$ and $\nu_e/\Omega_e \ll 1$. Both these conditions are reasonably well satisfied, and their maximum value is ≈ 0.3 for both conditions in the helium plasma at 175 G. Also, the low-frequency approximation $\omega/\Omega_i \ll 1$ is considered and in this case the maximum value is ≈ 0.1. Consequently, this approximation is well satisfied.

(v) In the calculation of the growth rate γ the larger quantities in the theory cancel leaving only smaller quantities, with the consequence that $\mathrm{Im}(\omega) = \gamma$ is subject to much larger error than the calculations for the $\mathrm{Re}(\omega)$.

When the theoretical dispersion relationship for $\mathrm{Re}(\omega)$ vs k_z is compared with the experimental results, reasonably good agreement is obtained. The comparison is shown in Figs. 7–10, where the full curve shows the numerically computed theoretical curve obtained by using the experimentally measured values for the zero-order parameters of the plasma. This good agreement is rather surprising in view of the approximations present in the theory and the possible errors present in the experimental results. The growth rate γ could not be measured directly, but its theoretically computed value is shown marked as the dashed curve in the figures, where its amplitude refers to the right-hand scale. It should be noted that this vertical scale changes from one figure to the next in order to obtain a convenient size plot. It is seen that for the $m = 1$ modes, in each case, that growth is predicted throughout the k_z range where oscillations were observed, although in some cases rather low growth rates were predicted [see Figs. 7(a) and 8(a)]. Also, the overlap between the predicted $m = +1$ and $m = +2$ growth rates shows that the $m = +2$ mode should take over for a smaller k_z value than that found experimentally. However, it was pointed out earlier that the predicted growth rates γ are subject to greater error than the $\mathrm{Re}(\omega)$ values.

Further, the experimental results obtained for the frequency variation as a function of neutral pressure (at constant magnetic field and axial wave number) in both gases show good agreement with the theoretically predicted values. Again, oscillations have been observed in the pressure range where a positive growth rate is predicted. However, below about 5-mTorr neutral pressure, values could not be obtained because multimode effects became apparent and turbulence set in at lower pressure values. This is to be expected from the high values of growth rate predicted by theory.

To conclude, the present results on the dependence of frequency ω and wave number k_z represent a comprehensive effort to identify the observed instability. The measurements have been performed in both helium and hydrogen afterglow plasmas at various field and neutral pressure values, and experiments have been performed in two plasma tubes in order to vary the radial density gradient. Comparison with the simple drift-dissipative theory in slab geometry shows reasonably good agreement. It would be desirable to compare the result with a theory calculated in full cylindrical geometry, including realistic boundary conditions. In spite of this, it is concluded that the observed instability is, indeed, the drift-dissipative instability.

[1]B. B. Kadomtsev, *Plasma Turbulence* (Academic, New York, 1965).
[2]A. B. Mikhailovski, Rev. Plasma Phys. 3, 159 (1967).
[3]C. W. Hartmann and R. H. Munger, in *Proceedings of the Conference on Physics of Quiescent Plasmas, Frascati*, 1967 (Consultants Bureau, New York, 1968), p. 181.
[4]P. F. Little and P. J. Barratt, Ref. 3, p. 173.
[5]H. N. Hendel, T. K. Chu, and P. A. Politzer, Phys. Fluids 11, 2426 (1968).
[6]L. Enriques, A. M. Levine, and G. B. Righetti, Plasma Phys. 10, 641 (1968).
[7]R. V. Aldridge and B. E. Keen, Plasma Phys. 12, 1 (1970).
[8]D. R. Pigache and G. N. Harding, Plasma Phys. 11, 805 (1969).
[9]S. C. Brown and D. J. Rose, J. Appl. Phys. 23, 711 (1952).
[10]S. J. Buchsbaum and S. C. Brown, Phys. Rev. 106, 196 (1957).
[11]A. V. T. Timofeev, Zh. Tekhn. Fiz. 33, 909 (1963) [Soviet Phys. Tech. Phys. 8, 682 (1964)].
[12]A. V. T. Timofeev, Dokl. Akad. Nauk. SSSR 152, 84 (1963) [Soviet Phys. Doklady 8, 890 (1964)].
[13]B. Agdur and B. Enander, J. Appl. Phys. 33, 575 (1962).
[14]R. L. Stenzel and R. W. Gould, Rev. Sci. Instr. 40, 1461 (1969).
[15]D. Smith, C. V. Goodall, and M. J. Copsey, J. Phys. B 1, 660 (1968).
[16]E. Blue and J. E. Stanko, J. Appl. Phys. 40, 4061 (1969).
[17]B. T. Dodo, Plasma Phys. 11, 800 (1969).
[18]F. F. Chen, Phys. Fluids 11, 811 (1968).
[19]T. K. Chu, B. Coppi, H. W. Hendel, and F. W. Perkins, Phys. Fluids 12, 203 (1969).
[20]T. Stix, Phys. Fluids 12, 627 (1969).
[21]T. H. Dupree, Bull. Am. Phys. Soc. 13, 263 (1968).

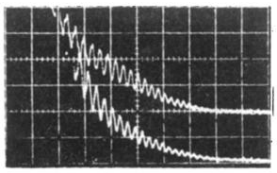

Helium plasma p = 20 m.torr
H = 500 gauss m = +1
ω = 3 kHz
Horizontal scale 1 msec/cm

FIG. 5. Typical decay curves for the instability, showing the output from two single probes separated azimuthally by 180°.